Magnetic Resonance in Medicine 56:463–468 (2006)

Factors Influencing Flip Angle Mapping in MRI: RF Pulse Shape, Slice-Select Gradients, Off-Resonance Excitation, and B_0 Inhomogeneities

Jinghua Wang,[1*] Weihua Mao,[4] Maolin Qiu,[1] Michael B. Smith,[4] and R. Todd Constable[1–3]

To understand the various effects that influence actual flip angles, and correct for these effects, it is important to precisely quantify the MRI parameters (such as T_1, T_2, and perfusion). In this paper actual flip angle maps are calculated using a conventional gradient-echo (GRE) sequence with different radiofrequency (RF) pulse shapes (Gaussian, sinc, and truncated-sinc), slice-selection gradients, off-resonance excitations, and B_0 field inhomogeneities. The experimental results demonstrate that RF pulse shapes significantly affect the flip angle distribution and calibration factors. Off-resonance RF excitations, B_0 nonuniformities, and slice-selection gradients can lead to degradations in the signal intensities of the images used to map the flip angle, and potentially introduce a bias and increased variance in the measured flip angles. Magn Reson Med 56: 463–468, 2006. © 2006 Wiley-Liss, Inc.

Key words: high-field MRI; RF uniformity; RF pulse; off-resonance excitation; selection gradient

Nonuniform effective flip angles across a slice in MRI may negatively influence the quantitative nature of the data produced by a given scan protocol. To increase the SNR in MR images, one can increase fill-factor by using a surface coil or phased-array coils, and/or increase the static magnetic field strength (1). However, both methods introduce new problems: the images become nonuniform as flip angle nonuniformities arise from the wave behavior of the RF pulses, RF penetration, eddy current, and/or coil configuration effects. The nonuniformities are not due to the usual spin characteristics of the object imaged (such as proton density, T_1, T_2, and perfusion), but to other characteristics such as imperfect hardware or the electromagnetic properties of the object. For quantitative MRI it is crucial to measure absolute flip angles and to correct the intensity nonuniformities that arise from these effects.

[1]Department of Diagnostic Radiology, Yale University School Medical Center, New Haven, Connecticut, USA.

[2]Department of Biomedical Engineering, Yale University, New Haven, Connecticut, USA.

[3]Department of Neurosurgery, Yale University School of Medicine, New Haven, Connecticut, USA.

[4]Center for NMR Research, Department of Radiology, Pennsylvania State University College of Medicine, Hershey, Pennsylvania, USA.

Grant sponsor: NIH; Grant numbers: NS40497; NS38467; EB00473; EB00454.

*Correspondence to: Jinghua Wang, Ph.D., Department of Diagnostic Radiology, Yale University, Anlyan Center, 300 Cedar Street, P.O. Box 208042, New Haven, CT 06520-8042. E-mail: Jinghua.wang@yale.edu

Received 8 December 2005; revised 23 March 2006; accepted 6 April 2006.
DOI 10.1002/mrm.20947
Published online 13 June 2006 in Wiley InterScience (www.interscience.wiley.com).

During RF excitation the slice profile, off-resonance, and B_0 effects give rise to variable precession angles of nuclear spins across an object. The slice profile follows a nonlinear relationship with flip angle according to the Bloch equations (2–4). A number of papers have discussed the correction and reduction of these factors through coil design (5), adiabatic pulse (6–8), and field mapping methods (9,10). However, few reports have quantitatively examined the influence of the RF pulse type and slice-selective gradients on the flip angles attained.

The flip angle is defined as the angle to which the net magnetization is rotated or tipped relative to the main magnetic field direction via the application of a RF excitation pulse at the Larmor frequency. Ernst and Anderson (11) long ago presented an expression for estimating the achieved flip angle in the case of small off-resonance excitation. To the best of our knowledge, however, no expression has been derived for estimating flip angles when the off-resonance excitation frequency is comparable to γB_1 (where B_1 is a magnitude of the RF pulse). If the flip angle mapping is influenced by off-resonance effects, this could have important implications for chemical shift imaging or quantitative fat imaging in vivo. It is also well known that B_0 inhomogeneities can influence the signal intensity of MR images; however, it is not clear whether B_0 inhomogeneities influence the absolute flip angle achieved. This study examines the impact of B_0 inhomogeneities on both the flip angle achieved and the calibration factor in vivo for gradient-echo (GRE) sequences.

THEORY

Measurement of Relative Flip Angles

GRE sequences with only a single excitation pulse are used in all of the experiments presented here in order to simplify the study of the factors that influence the measured flip angles. Conventional GRE sequences and segmented echo-planar imaging (EPI) GRE sequences are used to estimate the relative flip angles in phantom and in vivo studies. For a GRE sequence with excitation flip angle $\alpha(x)$, assuming that TR $\gg T_1$, the transmission field for noninteracting spins without transverse coherence can be written as (9,12–14):

$$\alpha_{actual} = \arccos(\lambda/2) \qquad [1]$$

where $\lambda = \frac{SI_2(x)}{SI_1(x)} = \frac{\sin\alpha_2(x)}{\sin\alpha_1(x)}$ is the ratio of signal intensities of two GRE images acquired with different excitation

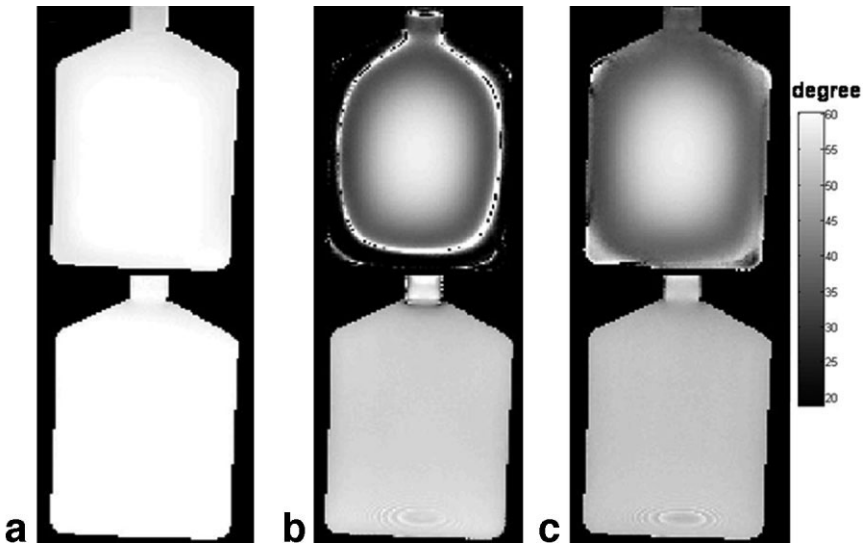

FIG. 1. Measured multislice flip angle map of a bottle phantom for sinc (column **a**), truncated-sinc (column **b**), and Gaussian (column **c**) RF pulses with (row 1) and without (row 2) slice-selective gradients at the nominal flip angle of 60°.

flip angles $\alpha_2(x) = 2\alpha_1(x)$ while TE and TR are kept fixed, and α_{actual} is the measured flip angle corresponding to the nominal (prescribed) flip angle of α_1.

Off-Resonance Excitation on the Precession Angle

For a hard pulse approximation, the averaged B_1^+ is calculated by

$$B_1^+ = \alpha_{actual}/(\gamma \cdot \tau) \quad [2]$$

where γ is the magnetogyric ratio, τ is the duration of the RF pulse, and B_1^+ is a positive circularly polarized component of B_1, which rotates in the same direction as the precession direction of nuclear spins. During the presence of the RF pulse, the nuclear spins precess around the effective field $B_{effective}$ (11):

$$B_{effective} = \sqrt{\frac{(\Omega_i - \omega_1)^2}{\gamma^2} + B_1^2} \quad [3]$$

where Ω_i is the Larmor frequency of spin i, and ω_1 is the frequency of the applied RF pulse with magnetic field B_1. When $|\Omega_i - \omega_1| \ll \gamma B_1$, then $B_{effective} \approx B_1$ and the flip angle can be estimated by Eq. [2]. Typically, RF pulse durations range from 2 to 10 ms. At 3 T, with an off-resonance frequency of 1 ppm (123 Hz), the flip angles begin to vary above 60° and a duration time of 10 ms or more. This suggests that the condition $|\Omega_i - \omega_1| \ll \gamma B_1$ is not satisfied even for small off-resonance effects of only 1 ppm at 3 T. With a pulse duration, τ, the total precession angle α_{total} about $B_{effective}$ should be given by

$$\alpha_{total} = \gamma \cdot B_{effective} \cdot \tau \quad [4]$$

MATERIALS AND METHODS

All imaging was performed on a Siemens 3 T Trio system with a Siemens head coil and a high-performance gradient system. The protocols for the human studies were approved by the Institutional Review Board of the Yale University School of Medicine.

Effects of Pulse Profile on Absolute Flip Angles

The RF pulse profile effects include the contribution of RF types and selection gradients. To investigate these effects

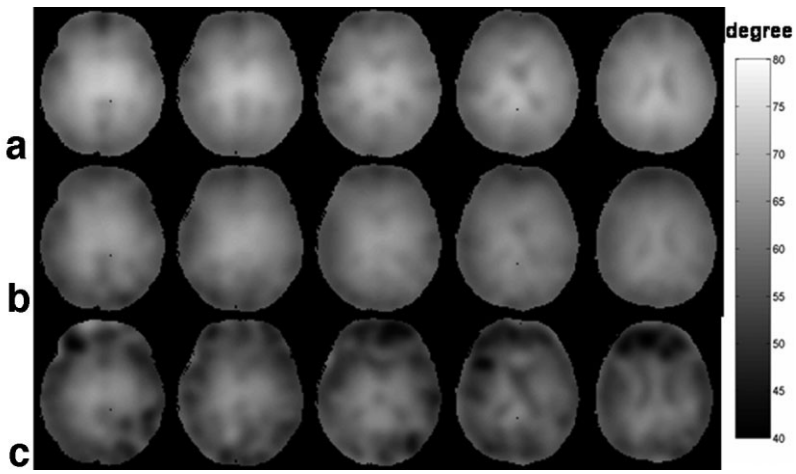

FIG. 2. Measured multislice flip angle map of the in vivo human brain for sinc (column **a**), truncated-sinc (column **b**), and Gaussian (column **c**) RF pulses at the nominal flip angle of 60°. Different columns represent different slices.

Table 1
Characteristics of RF Pulses*

	Averaged B_1	SD/mean (%)	R	Bandwidth (kHz)
Sinc	0.78	12	2.7	13.5
Truncated-sinc	0.73	12	10.24	20
Gaussian	0.68	25	5.120	10

*The averaged B_1 is normalized by the same duration time. SD is standard deviation of the measured field for a given RF pulse. R is the product of the bandwidth (frequency domain) and pulse duration time (time domain).

separately, a distilled water phantom of 113 × 40 × 160 mm^3 (length × width × height) doped with 10 mM $CuSO_4$ was used to estimate the influence of the RF profile on the measured flip angle with and without selection gradients. Three-dimensional (3D) images of the phantom were acquired using a conventional GRE sequence without selection gradients using different RF pulse shapes (sinc, Gaussian, and truncated-sinc profiles). The sinc, truncated-sinc, and Gaussian RF pulses had a duration/bandwidth of 2.000/13.5, 5.120/20, and 5.120/10 ms/kHz, respectively. Images were also acquired with selection gradients of different amplitudes using these RF pulses to evaluate the effects of selection gradients on the measured flip angles. The imaging parameters were TR/TE = 2000/5 ms, FOV = 200 × 200 mm^2, matrix = 112 × 128, slice number = 16 for the interleaved slice-selective acquisition or 16 per slab for the nonselective acquisition, and slice thickness = 3 mm. Both the selective and nonselective acquisitions were obtained with excitation flip angles of 30°, 45°, 60°, 90°, and 120° to estimate both the relative flip angles and the calibration factors.

For the in vivo studies, the relative flip angle and flip angle calibration factors were estimated using segmented EPI GRE acquisitions with excitation flip angles of 30°, 45°, 60°, 90°, and 120°, respectively. In vivo imaging was performed using sinc, truncated-sinc, and Gaussian pulse profiles to evaluate the effect of the RF pulse shape on the relative flip angles and calibration factors. Other acquisition parameters were TR/TE = 5000/16 ms, FOV = 240 × 210 mm^2, matrix = 128 × 112, slice thickness = 5 mm, 10 slices, bandwidth = 752 Hz per pixel, and seven segments. The same acquisition strategy was used for the in vivo measurements, but additional postprocessing for skull stripping was performed using a brain extraction tool developed by Smith (15).

Effects of Off-Resonance Excitation on Absolute Flip Angles

The distilled water phantom employed for RF pulse profile effects, was used to quantitatively evaluate the effect of off-resonance excitation on the measured flip angles. 3D images were obtained using a conventional GRE sequence with excitation flip angles of 30°, 45°, 60°, 90°, and 120° at offset frequencies ranging from 0 Hz to 800 Hz. The conventional GRE sequence with a nonselective rectangular RF pulse was used to minimize the effect of the slice profile on the absolute flip angles. The imaging parameters were TR/TE = 2000/20 ms, FOV = 200 × 200 mm^2, matrix = 128 × 128, slice number = 16 per slab, and slice thickness = 3 mm.

Effects of B_0 on Absolute Flip Angles

A spherical phantom, 17 cm in diameter, filled with distilled water and $NiSO_4.H_2O$ (1.25 g/l), was used to evaluate the effects of B_0 inhomogeneities on the measured transmit field map at TEs of 5, 10, 20 40, and 60 ms with flip angles of 30°, 45°, 60°, 90°, and 120°. The imaging parameters for B_0 mapping were TR = 1000 ms, TE = 8.5 and 11 ms, FOV = 200 × 200 mm^2, matrix = 256 × 256, slice number = 20, and slice thickness = 3 mm. The image parameters for relative flip angle and RF calibration factor were TR = 2000 ms, and matrix = 128 × 128. Other parameters were identical to those used for B_0 mapping.

RESULTS

Figure 1 shows relative multislice flip angle maps of a bottle phantom for sinc (column a), truncated-sinc (column b), and Gaussian (column c) RF pulses without (row 1) and with (row 2) slice-selective gradients at the nominal flip angle of 60°. The results indicate that hard RF pulses lead to significant differences in the relative flip angle maps and flip angle calibration factors compared to selective pulses. The measured flip angle calibration factors (slope of the measured flip angle vs. nominal flip angle) for the phantom were 0.93 for the sinc RF pulse, 0.68 for the truncated-sinc RF pulse, and 0.73 for the Gaussian RF pulse (row 1). The RF pulses in the presence of slice-selection gradients also produced different flip angle maps (row 2). These results demonstrate that the measured flip angle maps are significantly different for each of three RF pulse types, with or without slice-selective gradients.

Because flip angle mapping requires a long scan time for a 3D acquisition (several hours), it is not practical for estimating flip angle maps in 3D in vivo. To reduce the scan time, multislice flip angle maps in vivo were acquired with a segmented-EPI acquisition. The results for flip angle mapping using sinc (row a), truncated-sinc (row b), and Gaussian (row c), RF pulses at the nominal flip angle of 60° are shown in Fig. 2. The sinc-RF pulse produced the larg-

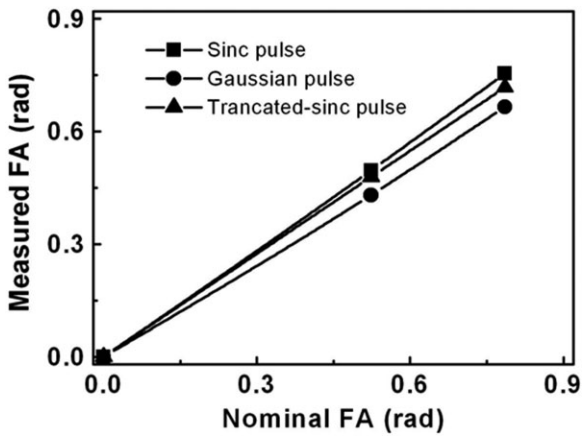

FIG. 3. Dependence of flip angle calibration factors in the human brain on the RF pulse types.

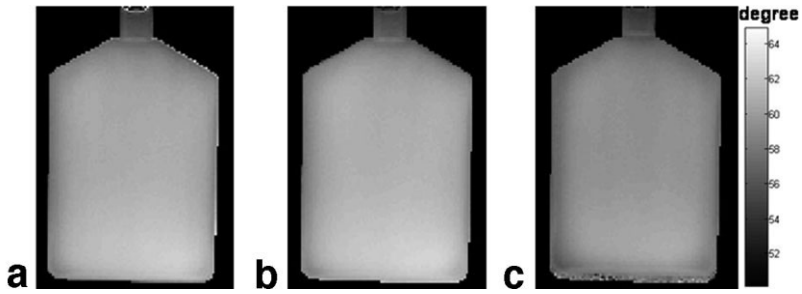

FIG. 4. Measured flip angle map of on-resonance (**a**) and 50 Hz (**b**) and 800 Hz (**c**) offset frequency excitation for a bottle phantom at the nominal flip angle of 60°.

est flip angle of the three pulse types, as shown by the bright regions in the center of the images in Fig. 2a. Figure 2b shows that the truncated-sinc RF pulse produced the most uniform flip angle distribution. The smallest net flip angle occurred with a Gaussian RF excitation pulse (Fig. 2c). In accordance with Eq. [2], the flip angle is proportional to B_1 under an approximation of hard pulses. The integration of B_1 over a fixed pulse duration is largest for the sinc shape, and smallest for the Gaussian shape at a given flip angle. Quantitative results are summarized in Table 1 (16), which shows that the extent of nonuniformity produced by these pulses is similar, with a standard deviation (SD) of 12%. The difference between the measured flip angle of the sinc RF and truncated-sinc RF pulses can be up to 6%. The maximum difference is significant because it is much larger than the error in the measured flip angle (around 2%), which is about twice the SNR (around 1%) of the images used to determine the flip angle.

The measured flip angle reflects only the mean relative flip angle across the object. For many applications it is important to know the absolute flip angle, and for this a flip angle calibration factor is required. The slope of the line in Fig. 3 for each RF pulse shape provides a calibration factor for in vivo imaging. The calibration factors are 0.96, 0.91, and 0.85 for the sinc, truncated-sinc, and Gaussian RF pulses, respectively.

Figure 4 shows the dependence of the measured relative flip angle map on the off-resonance excitation frequency. All images used to calculate the relative flip angle maps and flip angle calibration factors were acquired without selection gradients to avoid displacement artifacts. The relative flip angle maps in Fig. 4a–c are estimated on-resonance and at offsets of 50 and 800 Hz. Differences between the measured relative flip angle maps are $<2\%$ for the innermost slice, and $<4\%$ for the outermost slices.

Quantitative results for the calibration factors indicate that these factors changed $<1\%$ as a function of off-resonance frequency. As expected, increasing the frequency offset reduces the signal intensity and SNR, as shown in Fig. 5a. As the offset frequency increases, the signal intensity degrades, leading to increased errors in the measured flip angle, as shown in Fig. 5b.

Figure 6a shows the influence of B_0 inhomogeneities on the measured flip angle map at different TE's. The maximum inhomogeneities are less than ± 50 Hz for a water phantom. The signal intensities at TE's of 5 and 60 ms are shown in Fig. 6b and c. In the region of high B_0 field inhomogeneity the apparent measured flip angle approaches 60° because the ratio of image intensities in Eq. [1] approaches one as noise begins to dominate. In the limit of no signal the ratio approaches one because the noise is independent of flip angle. This is simply an SNR problem with the mapping measurement, and is not due to a direct B_0 influence on the flip angle achieved.

Figure 7 shows a function of measured averaged flip angles of a water phantom and their errors as TE. With the increasing TE from 5 to 60 ms, the variation in the averaged flip angles across the phantom is less than 2%, and this variation is not significant. However, the error of flip angles significantly increases with the increasing TE.

DISCUSSION

In vivo human studies illustrate that all RF pulses produce flip angles that vary spatially by $>10\%$ due to increasing wave behavior and RF penetration at 3T. The variable flip angles lead to nonuniform signal intensities. The nonuniform signal intensities may give rise errors in quantifying the MRI parameters (segmentation, T_1, T_2, and perfusion). Measuring absolute flip angles is a prerequisite for correcting signal inhomogeneities arising from these flip angle variations. Our results demonstrate that different RF pulse shapes induce differences in flip angles.

Equation [1] only provides the relative flip angle distribution across an object, and additional calibration of the RF transmitter is needed to improve absolute MR measure-

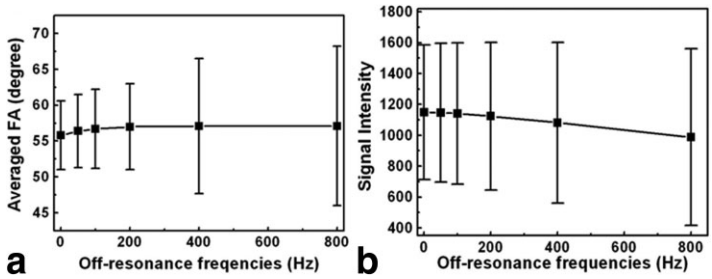

FIG. 5. Dependence of signal intensity (**a**) and the measured flip angle (**b**) on off-resonance excitation frequencies.

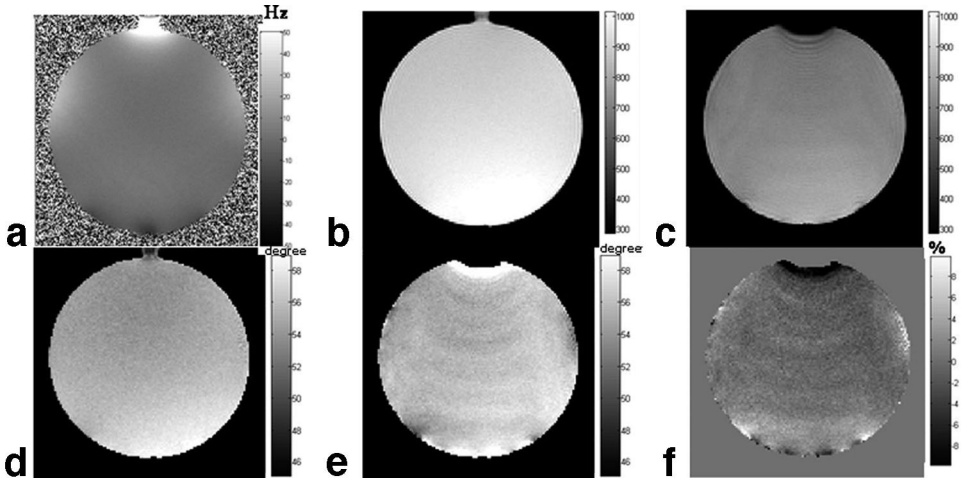

FIG. 6. Dependence of signal intensity and measured flip angle on inhomogeneous B_0 (**a**). The signal intensities (**b** and **c**) and measured flip angle maps (**d** and **e**) were obtained at TE = 5 and 60 ms, respectively. **f:** Percent difference of the measured flip angle maps.

ments. The calibration is affected by the coupling between the RF coil and the object, which is dependent on the coil loading, object position and size, and other parameters of the object. Consequently, it is necessary to calibrate the RF transmitter for each image acquisition in vivo.

Equation [2], which is used to calculate the average B_1^+, is valid only for hard pulses. For slice-selective pulses this formula is an approximation (12). Flip angle maps of a bottle phantom with or without slice-selective gradients indicated that slice-select gradients do not significantly impact the average flip angle values. However, the flip angle distributions are significantly different for the truncated-sinc (column b) and Gaussian (column c) RF pulses. Because the Bloch equations do not provide an analytical solution of slice profile for a general pulse, this approach for estimating flip angles may be useful for studying these effects in vivo at high field.

The results demonstrate that the RF pulse profile influences not only the distribution of the measured field, but also the flip angle calibration factor. Generally, in the presence of an RF pulse the total precession flip angle includes the contribution of elevation angle and azimuth angle, as shown in Eq. [4]. In the on-resonance condition, the flip angle is the angle to which the net magnetization is rotated or tipped relative to the main magnetic field direction via the application of a RF excitation pulse at the Larmor frequency. When off-resonance is small, the flip angle can be approximated to be the same as that for on-resonance (11). When off-resonance is comparable to or more than B_1, the definition of the flip angle is unclear. Figures 4 and 5 illustrate that off-resonance does not influence the average flip angle, but affects SNR and leads to errors in the measured flip angle.

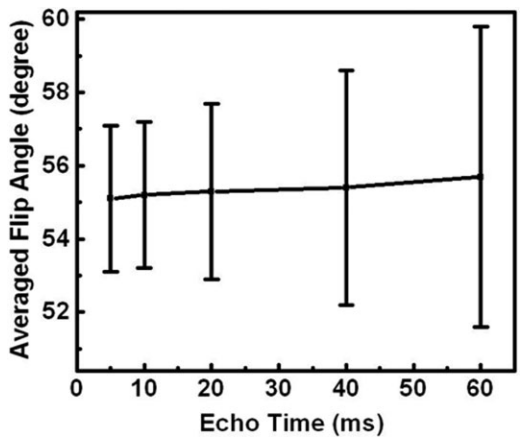

FIG. 7. Dependence of the measured flip angle on the different TEs.

It is well known that inhomogeneous B_0 leads to image distortions and signal loss with many pulse sequences. When images are acquired with a gradient echo sequence, the longer TE for the acquisitions can give rise to the stronger large influence of B_0 on the measured flip angles. The results in Figures 6 and 7 show that TE have a insignificant influence on the measured average flip angles of a water phantom. However, the errors in the measured flip angles significantly increase with the increasing TE. The flip angle mapping is sensitive to B_0 inhomogeneities if insufficient SNR is present in the images used to determine the flip angle map. If the signal intensities for one of the images used for flip angle mapping drops into the noise floor, then the ratio of the images will approach one, and the flip angle measured will approach 60° independently of the prescribed flip angle. However, there is no direct effect of B_0 on the flip angle achieved. These results are consistent with the off-resonance excitation and slice-selection gradients results. The slice-select gradient, B_0 inhomogeneities, and off-resonance excitation all reduce signal intensities in a similar manner, and differ only in terms of the magnitude and distribution of the response.

CONCLUSIONS

Experimental results from phantom and in vivo studies demonstrate that the RF pulse profile influences both the spatial uniformity of the flip angle achieved and the flip angle calibration factor. The RF pulse profiles used for flip

angle mapping, therefore, must be matched to the RF pulse shape used in the acquisition that is to be corrected by the mapping and calibration steps. Off-resonance effects, slice-selective gradients, and B_0 nonuniformities can impact the signal intensity of the measured images used for flip angle mapping, but do not directly influence the flip angles obtained.

ACKNOWLEDGMENTS

We thank Drs. de Graaf, Robin A, Hyeonjin Kim, and Chris M. Collins for helpful discussions.

REFERENCES

1. Edelstein WA, Glover GH, Hardy CJ, Redington RW. The intrinsic signal-to-noise ratio in NMR imaging. Magn Reson Med 1986;3:604–618.
2. Chan F, Pauly J, Macovski A. Effects of RF amplifier distortion on selective excitation and their correction by prewarping. Magn Reson Med 1992;23:224–238.
3. Maudsley AA, Matson GB. Selective excitation. In: Young IR, editor. Magnetic resonance imaging and spectroscopy in medicine and biology. Vol. I. New York: John Wiley and Sons; 1999. p 287.
4. Mulkern RV, Williams ML. The general solution to the Bloch equation with constant rf and relaxation terms: application to saturation and slice selection. Med Phys 1993;20:5–13.
5. Vaughan JT, Hetherington HP, Harrison JG, Otu JO, Pan JW, Pohost GM. High frequency volume coils for clinical NMR imaging and spectroscopy. Magn Reson Med 1994;32:206–218.
5. Norris DG, Haase A. Variable excitation angle AFP pulses. Magn Reson Med 1989;9:435–440.
6. Norris DG. Adiabatic radiofrequency pulse forms in biomedical nuclear magnetic resonance. Concepts Magn Reson 2002;14:89–101.
7. Tannus A, Garwood M. Adiabatic pulses. NMR Biomed 1997;10:423–434.
8. Ugurbil K, Garwood M, Rath A, Bendall MR. Amplitude and frequency/phase modulated refocusing pulses that induce plane rotations even in the presence of inhomogeneous B1 fields. J Magn Reson 1988;78:472–497.
9. Insko EK, Bolinger L. Mapping of radiology field. J. Magn Reson Ser A 1993;103:82–85.
10. Clare S, Alecci M, Jezzard P. Compensating for B(1) inhomogeneity using active transmit power modulation. Magn Reson Imaging 2001;19:1349–1352.
11. Ernst RR, Anderson WA. Applications of Fourier transform spectroscopy to magnetic resonance. Rev Sci Instrum 1966;37:93–102.
12. Wang J, Qiu M, Yang QX, Smith MB, Constable RT. Correction of transmission and reception fields induced signal intensity nonuniformities in vivo. Magn Reson Med 2005;53:408–417.
13. Stollberger R, Wach P. Imaging of the active B1 field in vivo. Magn Reson Med 1996;35:246–251.
14. Wang J, Qiu M, Constable RT. A method for rapid and effective correction of signal intensity nonuniformities with phased array coils in vivo. Magn Reson Med 2005;53:666–674.
15. Smith SM. Fast robust automated brain extraction. Hum Brain Mapp 2002;17:143–155.
16. de Graaf RA. In vivo NMR spectroscopy: principle and techniques. New York: John Wiley & Sons; 1998. p 187.